Supplementary Information

Aqueous Zinc-Ion Battery with an Organic-Inorganic Nanohybrid Cathode Featuring High Operating Voltage and Long-Term Stability

Saad Zafar, Muskan Sharma, Soumyasri Nikhilesh Mahapatra, Bimlesh Lochab*

Materials Chemistry Laboratory, Department of Chemistry, School of Natural Sciences, Shiv Nadar Institution of Eminence, Gautam Buddha Nagar, Uttar Pradesh 201314, India.

1. Materials and Methods

1.1. Materials: Ammonium vanadate (NH_4VO_3, Sigma Aldrich, 99%), amino-PEG-2-Amine (Broadpharm, 98%), hydrochloric acid (37%, Finar), zinc trifluoromethanesulfonate [Zn-($CF_3SO_3)_2$], and N-methyl-2-pyrrolidone (NMP, Finar), were used without further purification. Grafoil® paper and Celgard®-3501 was procured from Global Nanotech, India.

1.2. Synthesis of APA-NVO: The one-dimensional APA-NVO nanorods were prepared by a hydrothermal method. All the reagents used in this paper were analytically pure, and have never been further refined and processed. Firstly, ammonium vanadate (NH_4VO_3, 0.118 g) was dissolved in deionized water (H_2O, 20 ml) and stirred continuously. Then, 14 mmol Amino-PEG2-amine ($C_6H_{16}N_2O_2$) was added and stirred completely. The desired amount of hydrochloric acid (11.65 M, corresponding to a final pH values of 1, 2, 3, 4, 5) was added dropwise with vigorous stirring and pH was monitored using pH meter. After magnetic stirring, the yellow solution was transferred into a Teflon-lined stainless-steel autoclave, sealed and maintained at 120 °C for 6 h. After the hydrothermal treatment, the autoclave was cooled down to room temperature naturally and the precipitate was collected by vacuum filtration, washed with distilled water, and dried in vacuum at 80 °C. The final product was denoted as APA-NVO.

1.3. Characterization: The surface morphology and elemental mapping of the copolymer was examined using a field emission scanning electron microscope (FESEM), Jeol JSM-7610Plus coupled with an energy-dispersive X-ray (EDX, AMETEK) detector, under an acceleration voltage of 15 kV. Transmission electron microscopy (TEM) images were recorded using an HRTEM, JEOL-JEM-F200 instrument under an accelerating voltage of 200 kV, and d-spacing was calculated using GATAN software. Powder X-ray diffraction (PXRD) was recorded using a Bruker D8 diffractometer, using Cu Kα (λ = 1.5406 Å) in the scattering range (2θ) of 10–80° at

room temperature. FTIR spectra were recorded on a Nicolet iS20 spectrometer equipped with an interferometer, KBr/Ge-coated beam splitter, DTGS detector, and attenuated total reflectance diamond (iD5-ATR) accessory. Sixty-four scans at a resolution of 4 cm^{-1} were recorded in the range of 4000–400 cm^{-1}, averaged, and referenced against air. Thermogravimetric analysis (TGA) was recorded with a built-in gas controller (TGA2 SF/1100) and fitted with an XP1U TGA balance (ultra-microbalance) under a 50 mL/min flow rate of nitrogen and zero air in the temperature range of 35–800 °C at a heating rate of 10 °C/min. Raman spectroscopy measurements were carried out with an STR500 Airix microscope using a 532 nm laser at a power of 3 mW. X-ray photoelectron spectroscopy (XPS) measurements were carried out using a Thermo Fisher NEXSA surface analyzer with a monochromatized Al-Kα (1486.7 eV) radiation source to determine the chemical composition and binding energy (BE). The acquired spectrum was charge-corrected at a BE of carbon 1s peak at 284.6 eV and processed with the CasaXPS software.

1.4. Electrochemical testing: The electrochemical properties of APA-NVO4 nanorods are examined as a cathode material for ZIBs via CR2032-type coin cell assembled in open air under room temperature. The electrodes were prepared via a slurry-casting method. The active materials, conductive additive of Super P and binder of polyvinylidene fluoride (PVDF) in a weight ratio of 8:1:1 were mixed in 1-methyl-2-pyrrolidinone (NMP) to prepare the slurry. After being ground uniformly, the electrode slurry was coated onto a Grafoil® foils and dried under vacuum at 60°C overnight. The active mass loading is 2.9-3.2 mg cm^{-2}. The specific capacity of the electrode was calculated according to the total mass of active materials. A zinc plate, Celgard® (3501) and 3 M $Zn(CF_3SO_3)_2$ were used as the anode, separator and aqueous electrolyte, respectively. The cyclic voltammetry (CV) and electrochemical impedance spectroscopy (EIS) were carried out on the electrochemical workstation (BioLogic VMP3). EIS measurement was carried out at open circuit potentials with a frequency ranging from 200 MHz to 10 Hz. The rate performance was conducted in the voltage range of 0.1-2.0 V (vs. Zn^{2+}/Zn) at different current density. To monitor the electrode capability at higher current rates, the stability was tested at a high current density of 3.0 A g^{-1} for thousands of cycles.
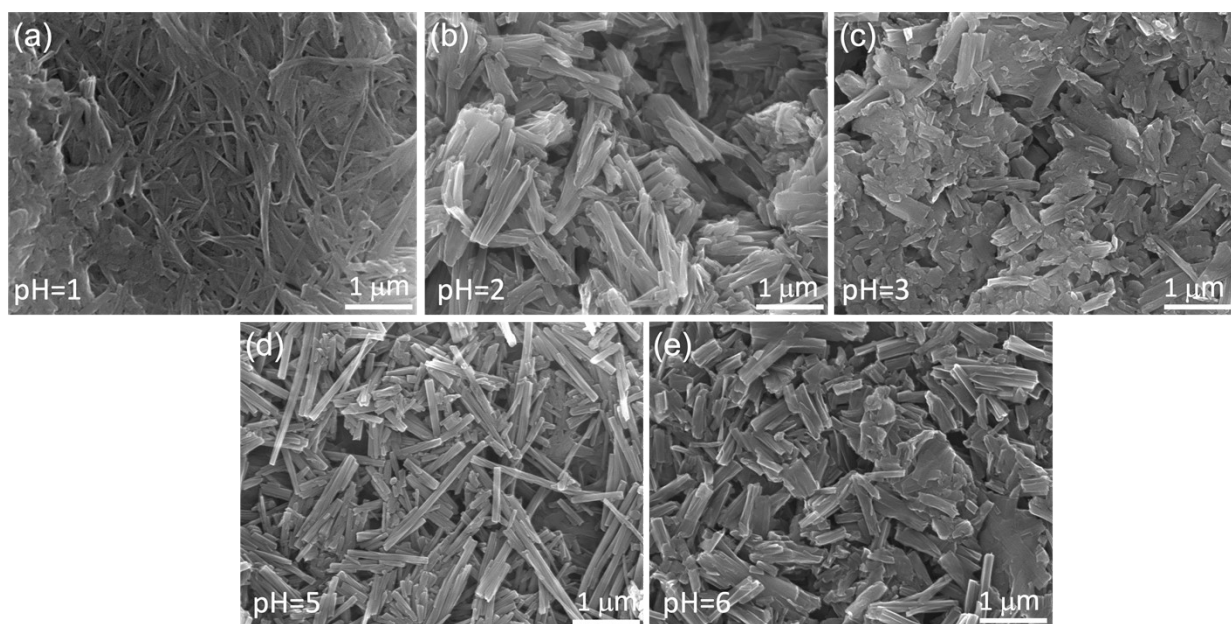
Figure S1. FESEM image of synthesized samples under different pH conditions. (a) pH=1, (b) pH=2, (c) pH=3, (d) pH=5, and (e) pH=6.
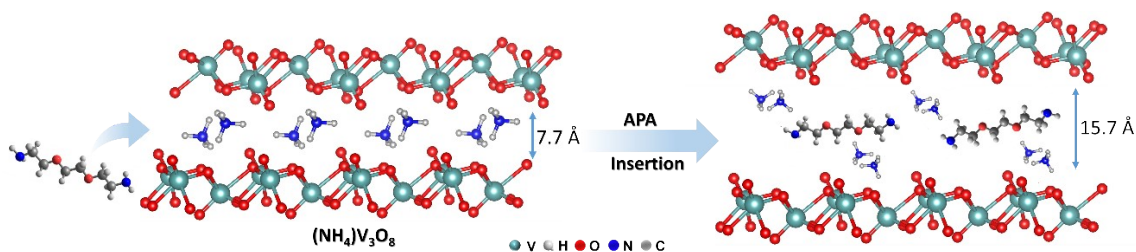
Figure S2. Probable mechanism of APA insertion into the NVO nanosheets. The structure is generated from the CIF file of JCPDS no. 41-0492, $NH_4V_3O_8 \cdot 0.5H_2O$ and plot by using VESTA software.

The effective intercalation of APA is due to favorable hydrogen bonding within the two layers of the NVO, linked *via* the oxygen of NVO layers and the amine and ether groups of APA to expand the NVO layered structure.

In our previous work,[1] computational studies suggested electronic interaction are favoured with the simultaneous H-bond formation between the N–H groups in APA with the surface O-atoms of the VO layers. The analysis of the charge density differences between the VO layers and the APA allowed us to determine the polarization of the electron density between the surface O-atoms of VO layers and the N–H bonds of the APA. Likewise, in present case similar interactions are possible not only with the N-H but also with the ammonium ions across the VO layer and the inserted APA molecules.
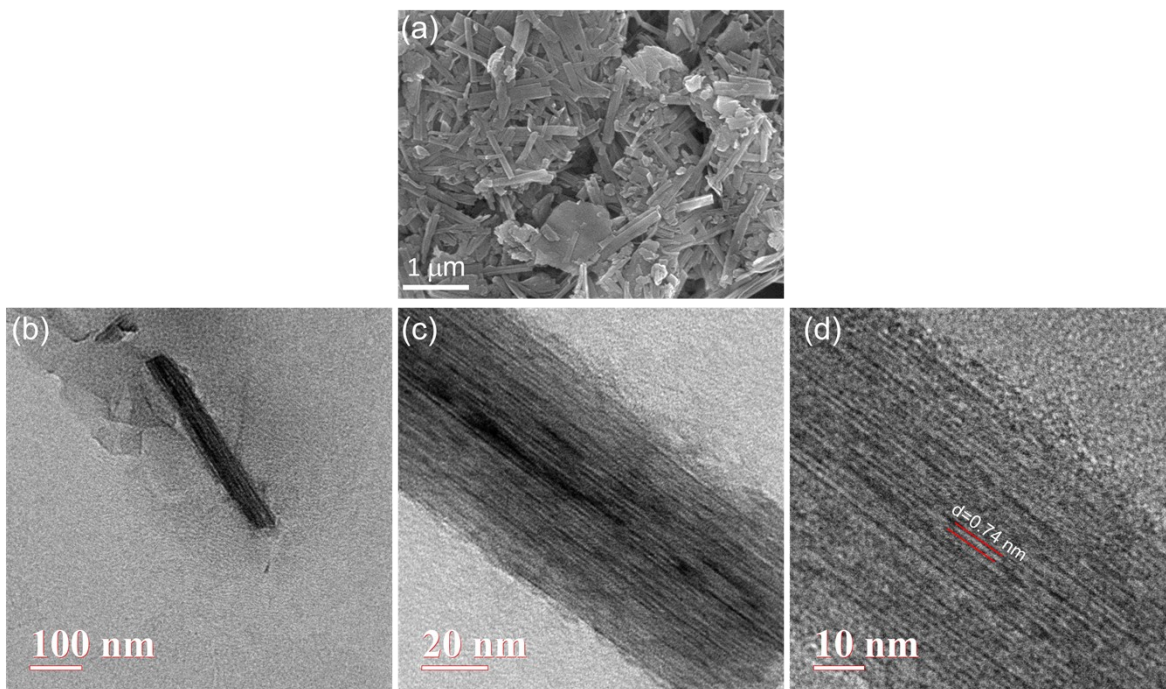

Figure S3. (a) FESEM, and (b-d) HRTEM image of NVO sample at different magnification.
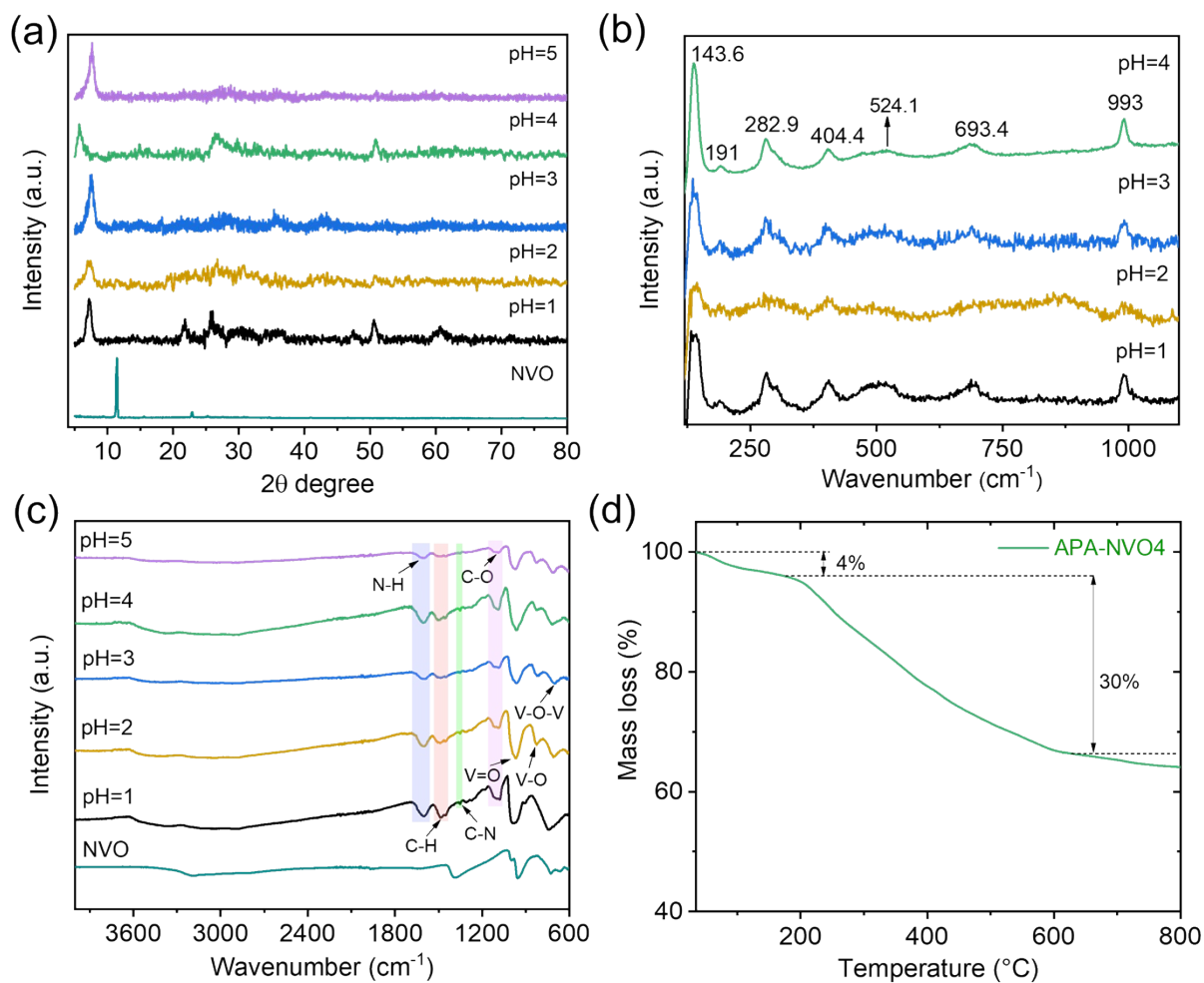
Figure S4. Characterization of APA-NVO nanorods. (a) XRD pattern, (b) FTIR spectrum, (c) Raman, and (d) TGA respectively.
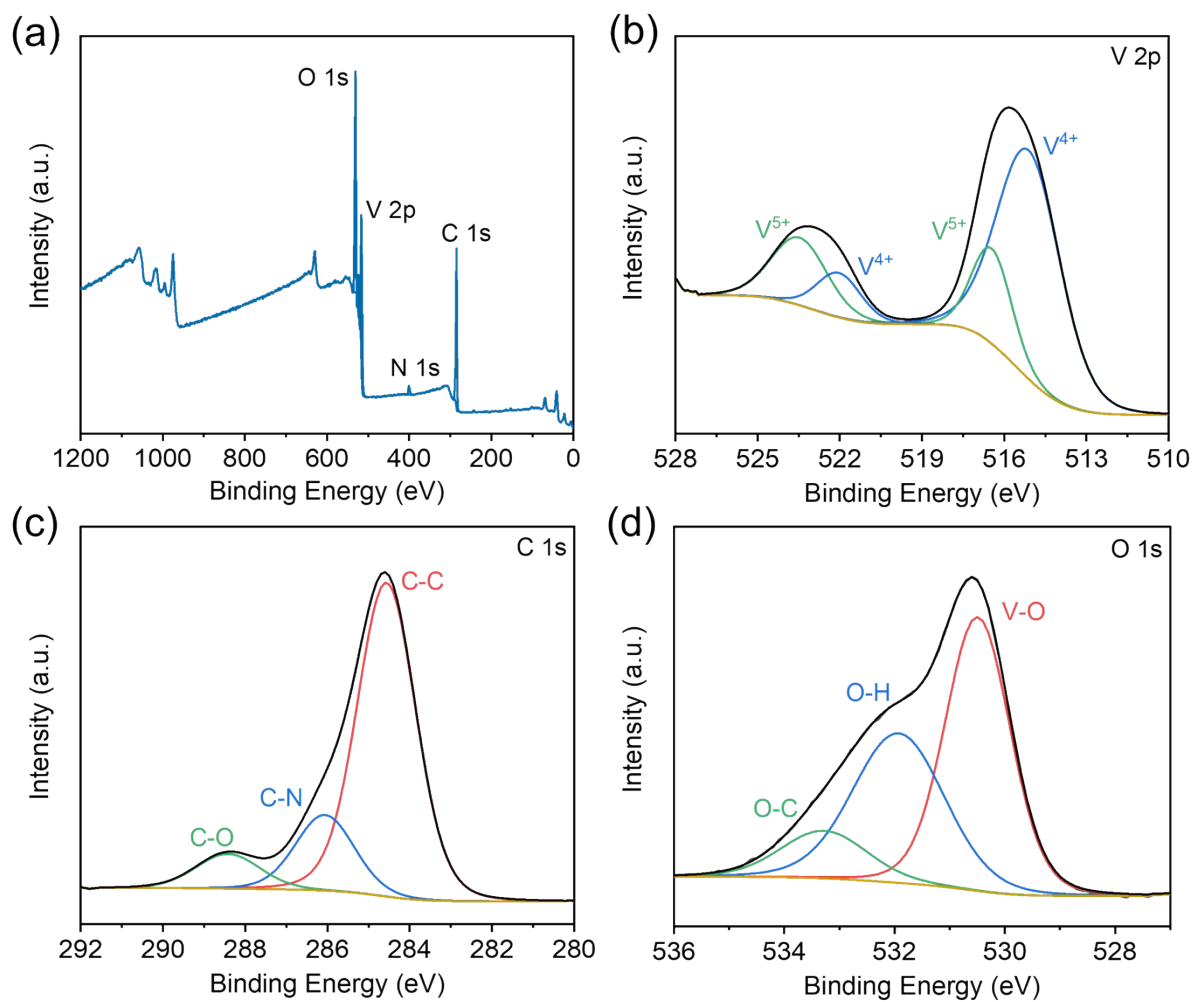
5

Figure S5. XPS spectrum of APA-NVO4. (a) wide survey spectra, High-resolution XPS spectra of (b) V 2p, (c) C 1s, and (d) O 1s.
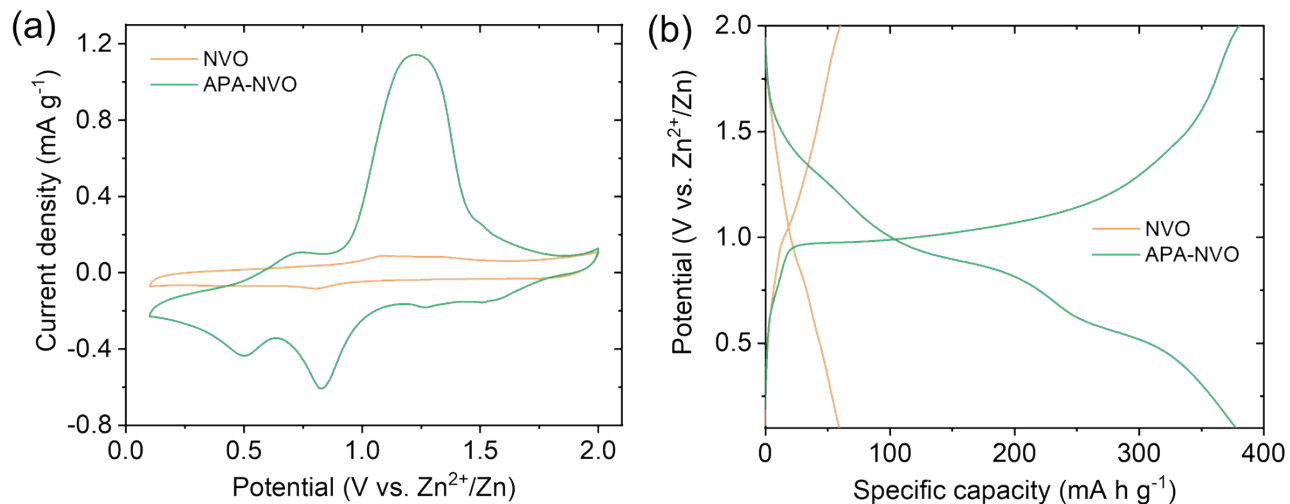
Figure S6. Electrochemical measurements of NVO, and APA-NVO4 for ZIBs. (a) CV curves at 0.2 mV s^{-1}, and (b) GCD curve of the ZIB at 100 mA g^{-1} current rate.
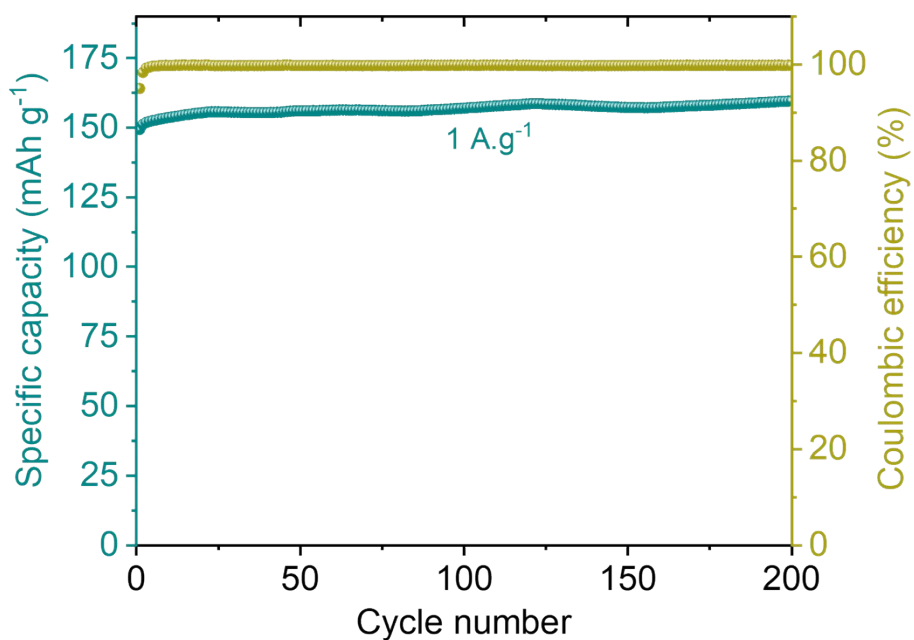

Figure S7. Electrochemical performance of APA-NVO4 for ZIBs showing cycling performance at 1 A g^{-1}.
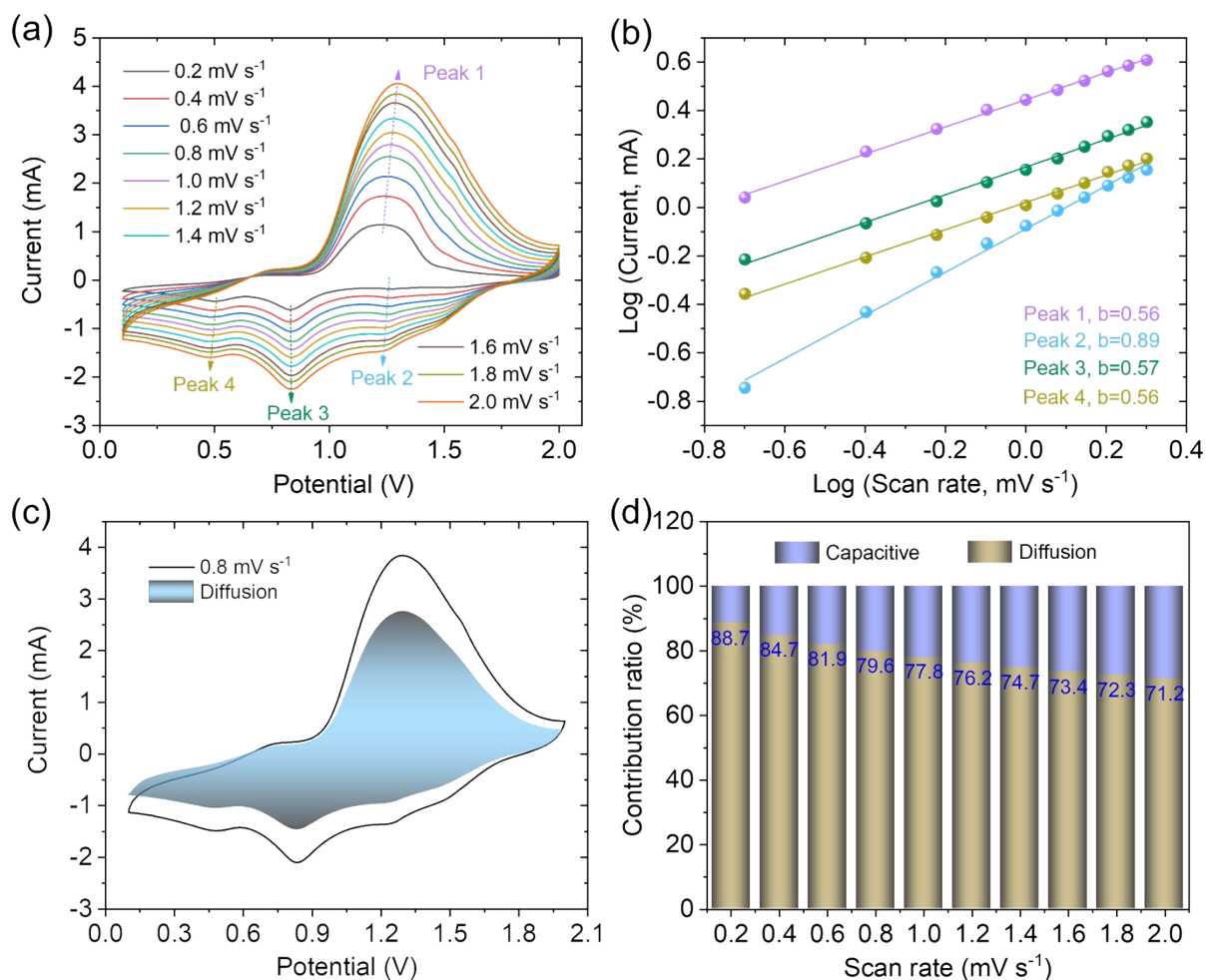
Figure S8. Kinetics analysis of APA-NVO4 nanorod. (a) CV curves of APA-NVO4 at various scan rates; (b) calculated b-values; (c) CV of APA-NVO4 with the diffusion dominating capacity contribution for the cathodic process at 0.8 mV s^{-1}; and (d) the proportion of capacity contributions at different scan rates.
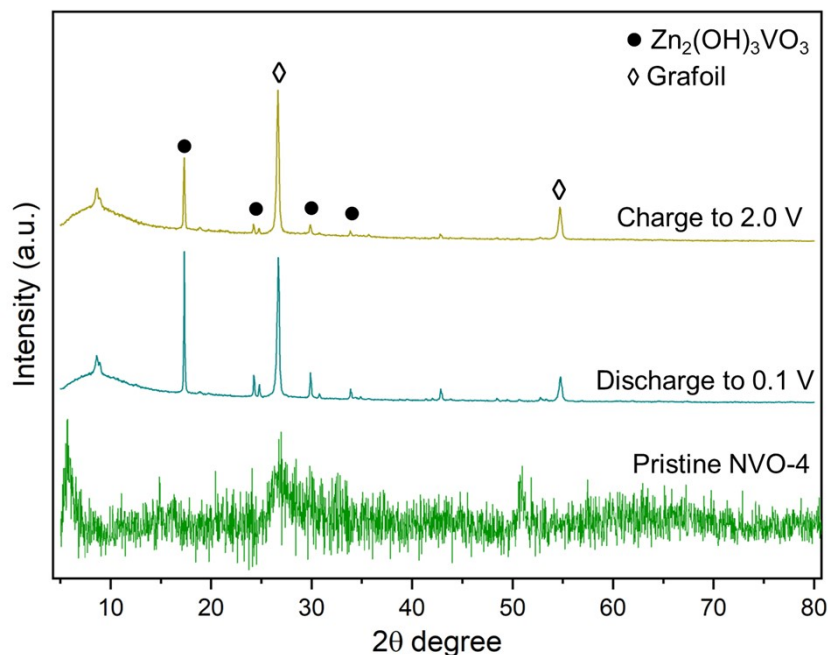
Figure S9. *Ex situ* XRD analysis of APA-NVO4 at discharge and charge state.

As shown in Figure S9, during the cycles of Zn^{2+} insertion/extraction, the diffraction peaks of $(NH_4)V_3O_8$ decreased in intensity and the peaks of $Zn_2(OH)_3VO_3$ appeared, revealing that the $(NH_4)V_3O_8$ undergoes an irreversible phase transformation and partly transformed to $Zn_2(OH)_3VO_3$. The layered structure of the VO-framework is not damaged during the Zn^{2+} ingress/egress as CV (Figure 2a) and charge/discharge curves (Figure 2b) of the $Zn//(NH_4)V_3O_8$ battery obviously remain unchanged. Then, the cathode materials in the $Zn//(NH_4)V_3O_8$ battery showed highly reversible and long cycle performance in ZIBs, as supported by the structure evolution after the cycles and cycling results in Figure 2e and Figure S7. To be specific, the characteristic peaks of cathode materials in the $Zn//(NH_4)V_3O_8$ battery shift toward higher 2θ angles with the discharge process.

When discharging to 0.1 V, these diffraction peaks have an obvious shift to the higher 2theta value, which indicates the shrinkage along the c-axis direction caused by electrostatic attraction accompanied by the cation insertion. After which the structure gets stabilized and has not changed further with the intercalation and deintercalation of Zn^{2+} during the further electrochemical process.

Also, in the charge phase of the electrode, we have observed evidence of Zn-composite formation, which is not fully deintercalated during the charging process. This further justifies and correlates with the kinetics data of zinc ion as shown in Figure S8 which shows a dominating diffusive contribution behavior of the cathode material.
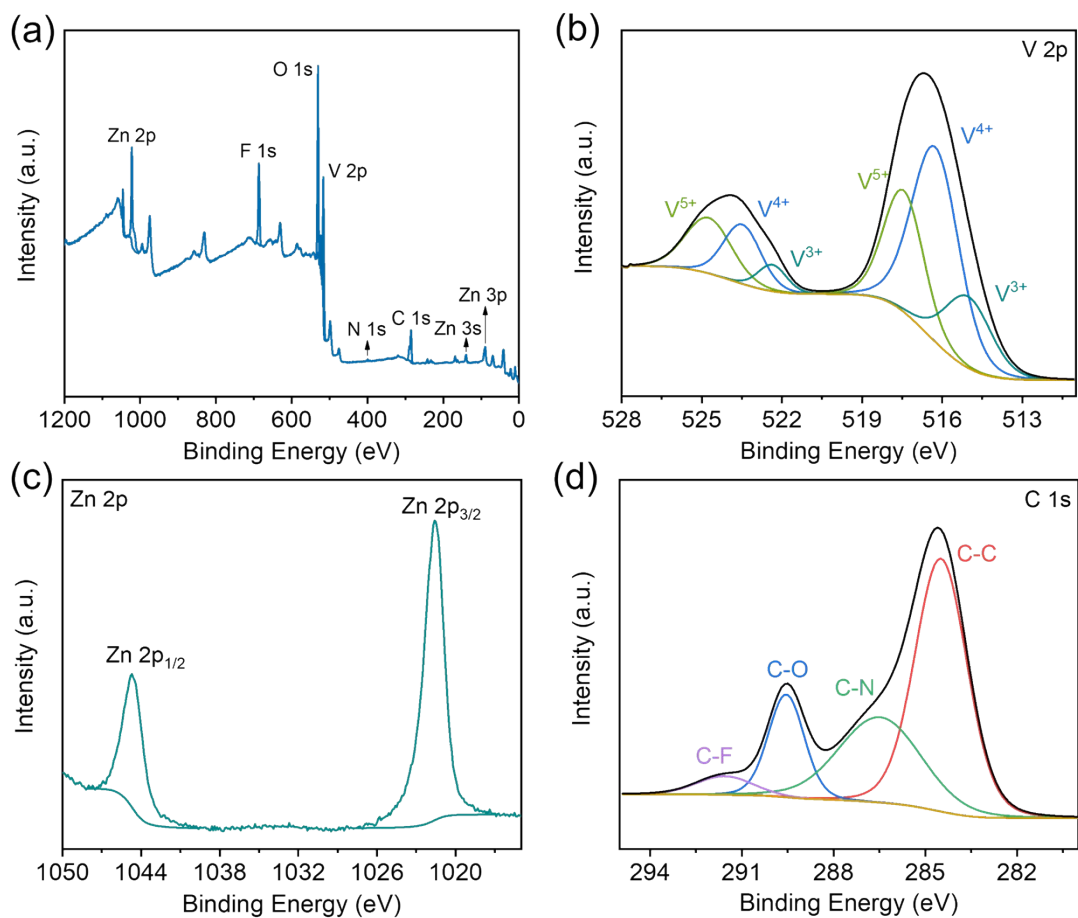
Figure S10. *Ex situ* XPS analysis of APA-NVO4; (a) wide-survey spectra; High-resolution XPS spectra of (b) V 2p; (c) Zn 2p; and (d) C 1s at discharge state.
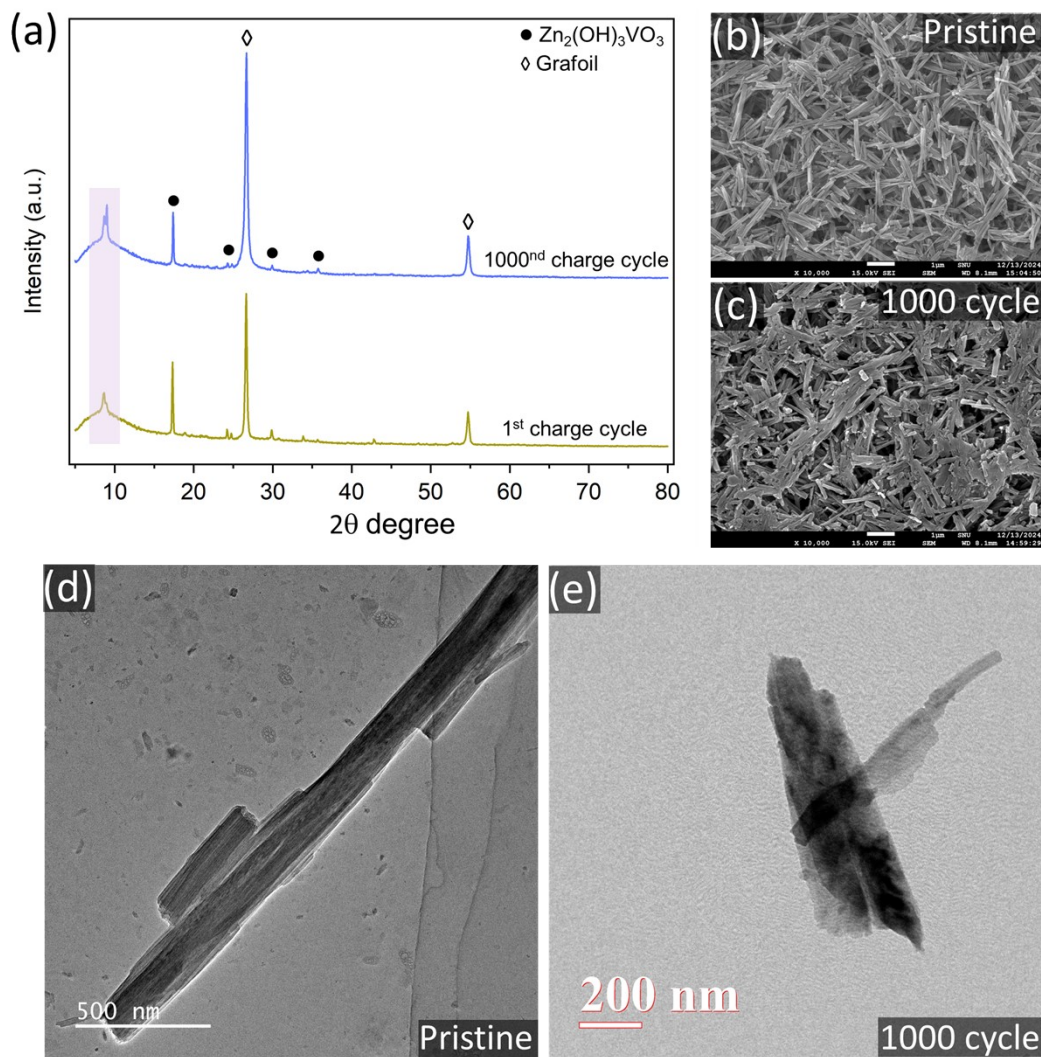
Figure S11. *Ex situ* analysis of APA-NVO4 after stability test, (a) XRD, (b-c) FESEM and (d-e) TEM images.

Table S1. Comparative performance of vanadium oxide-based cathodes in aqueous zinc-ion battery.

Material	Potential window (V)	Capacity (mAh g^{-1})/ A g^{-1}	Energy density (Wh kg^{-1})	Capacity value, Retention (%) (number of cycles)	Ref.
APA-NVO4	0.1–2.0	376.6 (0.1)	680	94%, 3 A g^{-1} (1200)	**This work**
V_2O_5	0.01–1.4	503 (0.1)	622	340, 0.5 A g^{-1} (700)	3
$Li_xV_2O5nH_2O$	0.4–1.4	470 (0.5)	423	192, 10 A g^{-1} (1000)	4
$VO_{20}.2H_2O$	0.4–1.1	423 (0.25)	177.7	182, 8 A g^{-1} (1000)	5
$V_2O_3@C$	0.3–1.5	350 (0.1)	220	90%, 5 A g^{-1} (4000)	6
V_6O_{13}	0.2–1.8	360 (0.2)	–	230, 4 A g^{-1} (2000)	7
$V_5O_{12}.6H_2O$	0.2–1.6	355 (0.5)	194	94%, 2A g^{-1} (1000)	8
$H_2V_3O_8$	0.2–1.6	394 (1/3C)	168	136.1, 5 A g^{-1} (1000)	9
$VS_4@rGO$	0.35–1.8	180 (1.0)	180	180, 1 A g 1 (165)	10
LiV_3O_8	0.2–1.6	298.4 (1.0)	~400	~200, 5 A g^{-1} (4000)	11
$Na0_{.33}V_2O_5$	0.2–1.6	367 (0.1)	–	218.4, 1 A g^{-1} (1000)	12
$K_2V_8O_{21}$	0.4–1.4	247 (0.3)	222.3	128, 6 A g^{-1} (300)	13
$Zn_{0.25}V_2O_5.nH_2O$	0.5–1.4	282 (1C)	~450 Wh L^{-1}	~81%, 8C (1000)	14
$Co_{0.247}V_2O_5.0.944H_2O$	0.6–2.2	432 (0.1	458.7	90.26%, 4 A g^{-1} (7500)	15
$Ba_{1.2}.V_6O_{16}.3H_2O$	0.3–1.4	346 (0.1)	260	95.6%, 5 A g^{-1} (2000)	16
$(NH_4)_2V_6O_{16}.1.5H_2O$	0.2–1.6	479 (0.1)	371.5	152, 5 A g^{-1} (3000)	17
$VOPO_4.xH_2O$	0.7–1.9	170 (0.1)	230	90, 2 A g^{-1} (500)	18

References.

1. S. Zafar, M. Sharma, K. Shai Mp, N. Karmodak, S. K. Singh and B. Lochab, *J. Mater. Chem. A*, 2024, DOI: 10.1039/D4TA01656D.
2. Y. Zhang, H. Jiang, L. Xu, Z. Gao and C. Meng, *ACS Appl. Energy Mater.*, 2019, **2**, 7861-7869.
3. M. S. Javed, H. Lei, Z. Wang, B.-t. Liu, X. Cai and W. Mai, *Nano Energy*, 2020, **70**, 104573.
4. Y. Yang, Y. Tang, G. Fang, L. Shan, J. Guo, W. Zhang, C. Wang, L. Wang, J. Zhou and S. Liang, *Energy Environ. Sci.*, 2018, **11**, 3157-3162.
5. D. Jia, K. Zheng, M. Song, H. Tan, A. Zhang, L. Wang, L. Yue, D. Li, C. Li and J. Liu, *Nano Res.*, 2020, **13**, 215-224.
6. Y. Ding, Y. Peng, S. Chen, X. Zhang, Z. Li, L. Zhu, L.-E. Mo and L. Hu, *ACS Appl. Mater. Interfaces*, 2019, **11**, 44109-44117.
7. W. Meng, R. Pigliapochi, P. M. Bayley, O. Pecher, M. W. Gaultois, I. D. Seymour, H.-P. Liang, W. Xu, K. M. Wiaderek, K. W. Chapman and C. P. Grey, *Chem. Mater.*, 2017, **29**, 5513-5524.
8. N. Zhang, M. Jia, Y. Dong, Y. Wang, J. Xu, Y. Liu, L. Jiao and F. Cheng, *Adv. Funct. Mater.*, 2019, **29**, 1807331.
9. P. He, Y. Quan, X. Xu, M. Yan, W. Yang, Q. An, L. He and L. Mai, *Small*, 2017, **13**, 1702551.
10. H. Qin, Z. Yang, L. Chen, X. Chen and L. Wang, *J. Mater. Chem. A,*, 2018, **6**, 23757-23765.
11. P. He, M. Yan, X. Liao, Y. Luo, L. Mai and C.-W. Nan, *Energy Storage Mater.*, 2020, **29**, 113-120.
12. P. He, G. Zhang, X. Liao, M. Yan, X. Xu, Q. An, J. Liu and L. Mai, *Adv. Energy Mater.*, 2018, **8**, 1702463.
13. B. Tang, G. Fang, J. Zhou, L. Wang, Y. Lei, C. Wang, T. Lin, Y. Tang and S. Liang, *Nano Energy*, 2018, **51**, 579-587.
14. D. Kundu, B. D. Adams, V. Duffort, S. H. Vajargah and L. F. Nazar, *Nat. Energy*, 2016, **1**, 16119.
15. L. Ma, N. Li, C. Long, B. Dong, D. Fang, Z. Liu, Y. Zhao, X. Li, J. Fan, S. Chen, S. Zhang and C. Zhi, *Adv. Funct. Mater.*, 2019, **29**, 1906142.
16. X. Wang, B. Xi, X. Ma, Z. Feng, Y. Jia, J. Feng, Y. Qian and S. Xiong, *Nano Lett.*, 2020, **20**, 2899-2906.
17. X. Wang, B. Xi, Z. Feng, W. Chen, H. Li, Y. Jia, J. Feng, Y. Qian and S. Xiong, *J. Mater. Chem. A*, 2019, **7**, 19130-19139.
18. H.-Y. Shi, Y. Song, Z. Qin, C. Li, D. Guo, X.-X. Liu and X. Sun, *Angew. Chem. Int. Ed.*, 2019, **58**, 16057-16061.